Screening and characterization of ternary oxides for high temperature carbon capture

Michael W. Gaultois,[1, a)] Matthew T. Dunstan,[1, a)] Adam W. Bateson,[1] Martin S. C. Chan,[2] and Clare P. Grey[1, b)]
[1)]*Department of Chemistry, University of Cambridge, Cambridge, CB2 1EW, United Kingdom*
[2)]*Department of Chemical Engineering and Biotechnology, University of Cambridge, Cambridge, CB2 3RA, United Kingdom*

Carbon capture and storage (CCS) is increasingly being accepted as a necessary component of any effort to mitigate the impact of anthropogenic climate change, as it is both a relatively mature and easily implemented technology. High-temperature CO_2 absorption looping is a promising process that offers a much lower energy penalty than the current state of the art amine scrubbing techniques, but more effective materials are required for widespread implementation. This work describes the experimental characterisation and CO_2 absorption properties of several new ternary transition metal oxides predicted by high-throughput DFT screening. One material reported here, Li_5SbO_5, displays reversible CO_2 sorption, and maintains ∼72 % of its theoretical capacity out to 25 cycles. The results in this work are used to discuss major influences on CO_2 absorption capacity and rate, including the role of the crystal structure, the transition metal, the alkali or alkaline earth metal, and the competing roles of thermodynamics and kinetics. Notably, this work shows the extent and rate to which ternary metal oxides carbonate is driven primarily by the identity of the alkali or alkaline earth ion and the nature of the crystal structure, whereas the identity of the e transition ion carries little influence in the systems studied here.

I. INTRODUCTION

The most expensive process in all carbon capture and sequestration strategies is the separation of CO_2 from waste streams, making the discovery of suitable materials for separation processes a critical step to achieving a neutral carbon footprint.[1] One technology that has shown recent promise is high-temperature CO_2 absorption looping, where a material first chemically reacts with CO_2 to form a solid carbonate phase which is then heated in a second reactor to decompose and release pure CO_2 and regenerate the starting material. Ca-based sorbents, such as limestone, are the most widely tested and used materials for this purpose,[2,3] and while being abundant and cheap, their CO_2 absorption capacity rapidly decays with use because of undesirable changes to the microstructure of the cycled $CaCO_3$ particles.[4]

The deficiencies in the CaO-$CaCO_3$ system have motivated the exploration of various alternative ternary metal oxide phases, including Li_2ZrO_3,[5,6] Na_2ZrO_3,[7,8] Li_4SiO_4,[9,10] Li_5AlO_4[11,12] and Li_5FeO_4.[13] In particular, the perovskite material $Ba_4Sb_2O_9$ was found to be able to carbonate reversibly with negligible capacity loss even after 100 cycles,[14] underlining the importance of searching for new materials with optimal CO_2 absorption properties.

Towards this goal, a previous study performed a large scale screening of the Materials Project database (www.materialsproject.org),[15] which contains the structural and theoretical ground state energies of over 67 000 solid state materials. After calculating the carbonation enthalpies of over 432 ternary oxide phases, a number of candidates with desirable predicted properties were synthesised and characterised to validate the screening method. While these experiments confirmed the relative accuracy of the screening methodology in predicting the reaction thermodynamics of the studied materials, they did not account for variations in kinetics or cycle stability, with many promising candidates such as Mg_6MnO_8, $Ca_4Nb_2O_9$ and Na_3SbO_4 failing on one or both of these requirements. Furthermore, while many promising candidates were obtained from the screening, most were not tested in this initial wave of experimental exploration and validation.

In this work, we used the results of the high-throughput DFT screening as the starting point for a more extensive experimental screening. 9 ternary metal oxide materials were prepared to investigate the role of crystal structure and chemical composition on the rate and reversibility of CO_2 absorption reactions. The predicted carbonation behaviour, CO_2 capacity and reaction are summarised in Table I. The entry for Li_6WO_6 was calculated directly from the Materials Project, as the initial screening omitted it due to the phase being unstable with respect to other phases in the phase diagram. The entry for Ca_3WO_6 was directly calculated in a similar fashion due to it being added to the database after the original screening.

The materials chosen here were selected for several reasons. Li_6MnO_4 and Li_6ZnO_4 have similarly high theoretical gravimetric CO_2 absorption capacities as Li_5AlO_4 and Li_5FeO_4 and can be regenerated at lower temperatures than the formerly studied materials, possibly allowing more efficient cycling. Li_2WO_4, Li_4WO_5, and Li_6WO_6 all lie in the complex Li–W–O phase diagram, where the existence of small energy differences between multiple stable phases may allow rapid and stable cycling between different phases during carbonation, much like the Li–Si–O system.[16] The materials from the Ca–W–O phase diagram, $CaWO_4$ and Ca_3WO_6, were chosen to determine the effect of changing the alkali element and how W substitution influences the CaO-$CaCO_3$ carbona-

[a)] these authors contributed equally
[b)] Electronic mail: cpg27@cam.ac.uk

TABLE I. Carbonation reactions and carbonation temperatures under $p_{CO_2} = 1 \times 10^4$ Pa of materials studied in this work, compared to the prototypical CaO sorbent. Carbonation temperatures were derived from ΔH and ΔS values largely determined by DFT calculations performed in a previous large scale screening of the Materials Project database[15] (values for Li_6WO_6 and Ca_3WO_6 were calculated as part of this study).

Compound	$T_{carbonation}$ (K)	CO_2 capacity ($g_{CO_2}/g_{sorbent}$)	Reaction
CaO	704	0.785	$CaO + CO_2 \longrightarrow CaCO_3$
Li_3SbO_4	532	0.213	$Li_3SbO_4 + CO_2 \longrightarrow LiSbO_3 + Li_2CO_3$
Li_5SbO_5	781	0.186	$Li_5SbO_5 + CO_2 \longrightarrow Li_3SbO_4 + Li_2CO_3$
Li_7SbO_6	903	0.165	$Li_7SbO_6 + CO_2 \longrightarrow Li_5SbO_5 + Li_2CO_3$
Li_6MnO_4	846	0.822	$\frac{1}{3}Li_6MnO_4 + CO_2 \longrightarrow \frac{1}{3}MnO + Li_2CO_3$
Li_6ZnO_4	821	0.450	$\frac{4}{7}Li_6ZnO_4 + CO_2 \longrightarrow \frac{1}{7}Li_{10}Zn_4O_9 + Li_2CO_3$
Li_6ZnO_4	817	0.772	$\frac{1}{3}Li_6ZnO_4 + CO_2 \longrightarrow \frac{1}{3}ZnO + Li_2CO_3$
Li_2WO_4	305	0.168	$Li_2WO_4 + CO_2 \longrightarrow WO_3 + Li_2CO_3$
Li_4WO_5	503	0.151	$Li_4WO_5 + CO_2 \longrightarrow Li_2WO_4 + Li_2CO_3$
Li_6WO_6	1005	0.137	$Li_6WO_6 + CO_2 \longrightarrow Li_4WO_5 + Li_2CO_3$
$CaWO_4$	323	0.153	$CaWO_4 + CO_2 \longrightarrow WO_3 + CaCO_3$
Ca_3WO_6	949	0.330	$\frac{1}{3}Ca_3WO_6 + CO_2 \longrightarrow \frac{1}{3}WO_3 + CaCO_3$

tion reaction. Li_5SbO_5 has a reasonable gravimetric capacity without requiring high temperatures for regeneration, and provides another point of reference for the role that Sb plays in CCS materials in light of previous work on Sb-containing ternary oxides, such as $Ba_4Sb_2O_9$.[14]

Taken as a whole, the selection of materials studied here allows us to study the impact of chemical, structural and thermodynamic factors on CCS performance, working towards the twin goals of materials discovery and increased fundamental understanding of structural evolution during carbonation. It also allows further validation of the original screening methodology to improve future studies.

II. METHODS

Materials were prepared using ceramic methods; stoichiometric amounts of solid precursor powders were ground together in an agate mortar and pestle, then reacted at high temperatures under air or argon. Owing to the wide range of materials, the same processing conditions could not be used for every materials; the precursors for each material, along with the processing schedule and atmosphere, are summarised in Table II. The reactions involving LiOH were pretreated at 423 K for 1 h in air to remove volatile components. Most complications in preparation or carbonation arose from melting of samples.

To analyse structural changes upon carbonation, a portion of the prepared material was subsequently annealed under a flow of pure CO_2 in a tube furnace at 973 K for 2 h (723 K for Li_4WO_5). Both the as-prepared and carbonated samples were characterised using room temperature powder X-ray diffraction (XRD), performed on a PanAlytical Empyrean diffractometer in Bragg-Brentano geometry using Cu K_α radiation. The instrument contributions to the peak shape were determined using a diffraction pattern of NIST SRM Si 640c collected in a separate measurement. Rietveld and Pawley refinement were performed using the Topas software package.[17] *In situ* XRD measurements above room temperature were performed using an Anton-Paar XRK 900 furnace, with a total gas flow rate of 100 mL min^{-1}.

The carbonation and regeneration reactions of the screened materials were investigated with thermogravimetric analysis (TGA) (TGA/DSC 1, Mettler Toledo) operating at atmospheric pressure. In each experiment, a sample of ∼20 mg of powder was placed in a 70 μL Al_2O_3 crucible, supported on a cantilever-type balance. The reaction chamber was heated by a tube furnace surrounding the balance. Both the protective gas and the purge gas were N_2, and were fed to the TGA reaction chamber from a common source with a total flow rate of 100 mL min^{-1}. The reactive gas was either N_2 or CO_2, fed by a capillary so that the gas could flow over the top of the crucible. The partial pressure of CO_2 at the surface of the solid sample was adjusted by varying the mix of N_2 and CO_2 in the reactive gas, while keeping a constant overall flow rate of 100 mL min^{-1}. The supply of reactive gas was controlled by solenoid valves, allowing automatic changing of reactive gas at different points within the TGA program. The actual CO_2 concentration at the gas-solid interface was calibrated against the well-understood thermodynamic CaO/$CaCO_3$ carbonation equilibrium. Over a range of different p_{CO_2}, the temperature of the onset of $CaCO_3$ decomposition was recorded and the corresponding CO_2 partial pressure in contact with the solid phase was determined from the phase diagram of the CaO–$CaCO_3$–CO_2 system.

TABLE II. List of precursor materials and processing schedules used during the solid-state preparation of the screened CCS materials.

CCS material	Precursor materials	Reaction programme	Atmosphere
Li_5SbO_5	LiOH and Sb_2O_5	973 K for 24 h, 1073 K for 12 h	argon
Li_6MnO_4	Li_2O and MnO	1223 K for 12 h	argon
Li_6ZnO_4	LiOH and ZnO	973 K for 24 h, 1073 K for 12 h, 1173 K for 24 h	argon
Li_2WO_4	LiOH and WO_3	973 K for 12 h	argon
Li_4WO_5	Li_2O and WO_3	973 K for 12 h, 1073 K for 12 h	argon
Li_6WO_6	Li_2O and WO_3	973 K for 48 h	air
$CaWO_4$	$CaCO_3$ and WO_3	1273 K for 12 h	air
Ca_3WO_6	$CaCO_3$ and WO_3	1273 K for 48 h	air

For single cycle carbonation and regeneration TGA experiments, the material was heated from 323 K to 973 K at a rate of 10 K min^{-1}, and then held at 973 K for 120 min. In the case of Li_6ZnO_4 this temperature was held for only 10 min. In the case of Li_4WO_5, the maximum temperature used was 732 K. In each case CO_2 was supplied as the reactive gas for the duration of the experiment. For the multiple cycling experiments of Li_5SbO_5, Li_6WO_6 and Li_4WO_5, the material was heated isothermally at 973 K (723 K for Li_4WO_5) for 60 min under $p_{CO_2} = 1.05 \pm 0.12 \times 10^5$ Pa, then heated to 1223 K (823 K for Li_4WO_5) and held at that temperature for 40 min under pure N_2, before being cooled to 973 K (723 K for Li_4WO_5) and held for 20 min under N_2. This sequence was repeated for 25 cycles of carbonation and regeneration. The samples obtained at the end of these cycles were characterised using room-temperature XRD as described above, along with other samples cycled in a tube furnace for 3 cycles, with a program of carbonation at 973 K for 2 h under pure CO_2 followed by regeneration at 1223 K for 2 h under pure N_2 (temperatures of 723 K and 823 K were used for Li_4WO_5).

Backscattered electron micrographs were collected using a field emission gun scanning electron microscope (Camscan MX2600) operating at an accelerating voltage of 10 kV. 10 nm of Pd was sputter-deposited on specimens to minimize charging.

The porosity and specific surface area (SSA) of the candidate materials were determined using volumetric sorption measurements (TriStar3000 analyzer, Micromeritics) in N_2 at 77 K. The SSA was calculated using Brunauer-Emmett-Teller (BET) analysis using N_2 adsorption.[18]

III. RESULTS AND DISCUSSION

A. Characterisation of screened materials

XRD was used to characterise the identity and purity of all materials, which were single-phase after preparation with the exception of Li_6MnO_4. Despite multiple different synthetic approaches, Li_6MnO_4 could not be produced without the persistence of significant amounts of MnO and Li_2CO_3 (see Supporting Information). The material was still included in the initial thermogravimetric experiments, as Li_6MnO_4 and the impurities are expected to participate in the carbonation reactions.

The powder patterns of all materials and mixtures were well-fit by the structural models, except Li_6WO_6. The average crystal structure of Li_6WO_6 ($Immm$) is described by half-filled edge-sharing WO_6 octahedra extending along the *b* direction, and corner-sharing along the *c* direction (Figure 1). The measured diffraction pattern of Li_6WO_6 contains sharp reflections well-modelled by the $Immm$ spacegroup, along with several additional broad reflections with Warren-type lineshapes, beyond the expected reflections (Figure 1). This is consistent with the original report by Hauck, where extra reflections were attributed to partial ordering of W^{6+} ions[19] in the formally half-filled $2a$ site. This is sensible in light of Pauling's rules, where structures will seek to maximize the distance between highly charged centres to minimize the Coulombic energy penalty. In this case, given the high charge-radius ratio of W^{6+}, it is energetically-unfavourable to form edge-sharing pairs of WO_6 octahedra, and W^{6+} orders on the $2a$ site (at least locally) to minimize the system energy.

The surface area of the candidate materials was characterised using BET (see Supporting Information); all materials exhibit low surface areas ($\sim$1 m^{2}g^{-1}), which is expected as the ceramic methods used in the material preparation involve annealing at high temperatures for long dwell times. Owing to the similar, low surface areas, we do not expect sample morphology or surface area to be a factor in the relative performance of the pristine materials studied here.

Analysis of the materials after carbonation using room-temperature XRD confirm the following reactions take place (diffractograms shown in Supporting Information):

$$Li_5SbO_5 + CO_2 \longrightarrow Li_3SbO_4 + Li_2CO_3 \quad (1)$$

$$\frac{1}{3}Li_6MnO_4 + CO_2 \longrightarrow \frac{1}{3}MnO + Li_2CO_3 \quad (2)$$

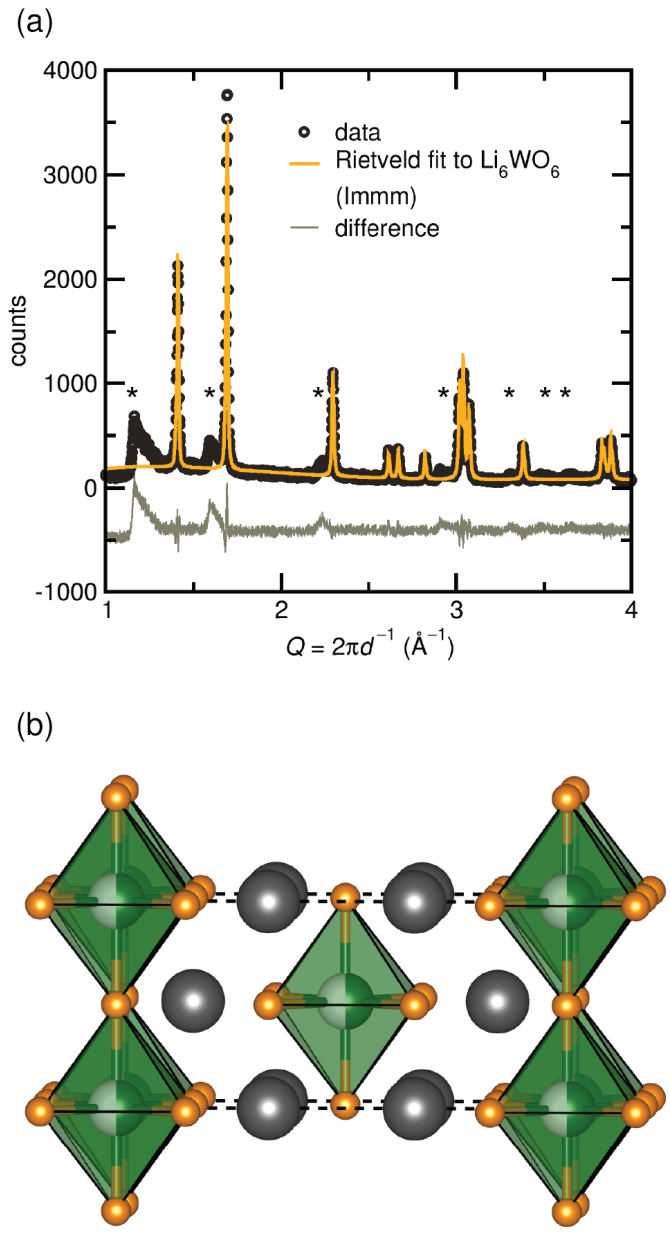

FIG. 1. (a) XRD pattern and Rietveld refinement of Li_6WO_6 in the $Immm$ spacegroup ($\lambda = 1.5405$ Å). Additional peaks with Warren-type broadening (*) are present due to ordering of W^{6+} ions in the half-filled $2a$ site. It is energetically unfavourable to have edge-sharing octahedra, which would bring together highly-charged W^{6+} ions. Ordering of W to prevent edge-sharing WO_6 pairs in the local structure lowers the system energy, and leads to the broadened extra reflections observed in the XRD pattern. (b) The average crystal structure of Li_6WO_6 ($Immm$) is described by half-filled edge-sharing WO_6 octahedra extending along the *b* direction, and corner-sharing along the *c* direction.

$$\frac{1}{3}Li_6ZnO_4 + CO_2 \longrightarrow \frac{1}{3}ZnO + Li_2CO_3 \quad (3)$$

$$Li_4WO_5 + CO_2 \longrightarrow Li_2WO_4 + Li_2CO_3 \quad (4)$$

$$Li_6WO_6 + CO_2 \longrightarrow Li_4WO_5 + Li_2CO_3 \quad (5)$$

These results agree with the predicted carbonation reactions obtained from the Materials Project screening (Table I), with several exceptions. First, $CaWO_4$, Ca_3WO_6 and Li_2WO_4 showed no evidence of carbonation in their diffractograms following exposure to flowing CO_2 in a tube furnace, and were thus not subjected to any further experiments. Second, we observe that Li_6ZnO_4 carbonates to form ZnO and Li_2CO_3, rather than the products predicted by the screening ($Li_{10}Zn_4O_9$ and Li_2CO_3). This was more carefully confirmed by performing *in situ* XRD at 10 minute intervals during carbonation of Li_6ZnO_4 in atmospheres of 100% CO_2 and 50% $CO_2(N_2)$, at 50 K intervals between 773 K and 973 K; there was no evidence for the formation of $Li_{10}Zn_4O_9$ nor other Zn species. Further, XRD measurements on Li_6ZnO_4 powder exposed to ambient lab atmosphere for prolonged periods revealed the presence of only Li_6ZnO_4, ZnO, and Li_2CO_3.

For each material in the Materials Project, our screening methodology finds several different possible carbonation reactions, and ranks them based on the calculated carbonation enthalpy of each reaction. We select the reaction with the lowest (most negative) carbonation enthalpy and assume that it will be the only reaction that is activated.

Selecting the reaction with the lowest carbonation enthalpy works well when there is a reaction that is clearly more favourable than the other possibilities, but in this case the two reactions have extremely similar carbonation enthalpies, well within the errors of the underlying DFT methodology:

$$\frac{1}{3}Li_6ZnO_4 + CO_2 \longrightarrow \frac{1}{3}ZnO + Li_2CO_3 \quad (6)$$
$$\Delta H = -2.25\,\text{eV}(-217\,\text{kJ mol}^{-1})$$

$$\frac{4}{7}Li_6ZnO_4 + CO_2 \longrightarrow \frac{1}{7}Li_{10}Zn_4O_9 + Li_2CO_3 \quad (7)$$
$$\Delta H = -2.26\,\text{eV}(-217\,\text{kJ mol}^{-1})$$

Selecting the reaction with the lowest carbonation enthalpy also neglects kinetic limitations, which are likely responsible for the inert behaviour of $CaWO_4$, Ca_3WO_6 and Li_2WO_4 seen here. These kinetic considerations cannot be easily treated from thermodynamic quantities such as ΔH and ΔS calculated from the Materials Project.

B. Initial carbonation reaction thermogravimetry

To investigate the initial carbonation capacity and kinetics of the candidate materials, ramp TGA experiments were carried out at a rate of 10 K min^{-1} (Figure 2). The experimental capacities and reaction temperatures for the initial carbonation step compared to the theoretical values from the Materials Project screening are summarised in Table III.

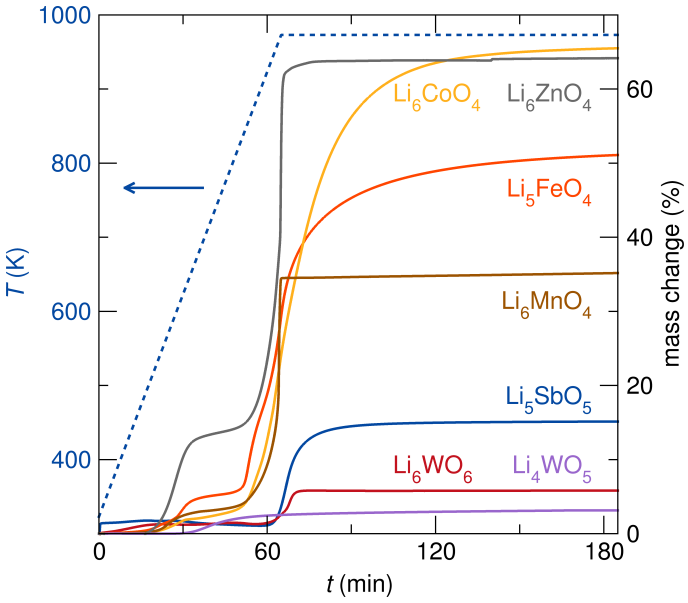

FIG. 2. TGA traces for selected candidate materials heated under CO_2 ($p_{CO_2} = 1 \times 10^4$ Pa). Most materials studied here exhibit similar carbonation profiles, with the onset of a small initial mass gain at low temperature around ∼600 K followed by a sharp onset and substantial mass gain initiated between 850 K and 900 K. Traces from previous studies for Li_5FeO_4 and Li_6CoO_4 are added for comparison[15] .

The initial TGA experiments are consistent with the $T_{carbonation}$ values obtained from the screening; the majority of materials lie within ∼100 K of their experimental values. This corresponds to an error of ∼10 meV, and is well within the limits of the DFT methodology. However, the experimental carbonation capacities are all lower than the corresponding theoretical limits, with some materials showing significant deviations (*e.g.* Li_6MnO_4, Li_4WO_5, and Li_6WO_6).

It is clear from the TGA ramp experiments that Li_6MnO_4 and Li_6ZnO_4 exhibit a two-stage carbonation behaviour, commonly observed in other materials with a similar chemical composition and structure such as Li_5AlO_4, Li_5FeO_4, and Li_6CoO_4.[11,13,15] This two-stage carbonation features the onset of a small initial mass gain at low temperature around ∼600 K followed by a sharp onset and substantial mass gain initiated between 850 K and 900 K. The low-temperature regime is ascribed to reactions near the surface, whereas the high sorption of CO_2 in the high-temperature regime is ascribed to bulk solid-state reaction, enabled by a sufficiently high rate of ionic transport activated at higher temperatures.

C. Cycling experiments

Of the materials that could initially carbonate, only Li_5SbO_5, Li_4WO_5 and Li_6WO_6 could be regenerated and cycled in the TGA. Li_6ZnO_4 and Li_6MnO_4 both show evidence of melting at the higher temperatures required for regeneration, most likely due to the formation of Li_2CO_3 (with a melting point of 996 K), making them unsuitable for further use.

The materials that could be regenerated were cycled 25 times in the TGA; mass–time curves for the 1st, 2nd, 10th and 25th cycles are shown in Figure 3. The difference in mass after 60 minutes of exposure to CO_2 at reaction temperature was used to determine the mass of CO_2 absorbed, which was then used calculate the percentage of theoretical capacity according to the appropriate reaction stoichiometry shown earlier in Equations 1–5. The CO_2 sorption capacity as a percentage of theoretical capacity for the material is plotted as a function of cycle number, along with the corresponding performance of CaO for comparison (Figure 4).

Li_5SbO_5 displays an initial carbonation capacity >90% of the theoretical capacity, and while this quickly decreases to ∼75% by the 3rd CO_2 sorption/desorption cycle, Li_5SbO_5 displays excellent capacity retention for the duration of the cycling experiment (Figure 4), with ∼72% of the theoretical capacity after 25 cycles. Furthermore, in addition to the small decrease in capacity with cycling, the material shows much slower carbonation kinetics. In the first cycle, Li_5SbO_5 absorbs 70% of the theoretical capacity of CO_2 within 5 minutes when exposed to CO_2, whereas achieving the same sorption after 10 cycles takes 60 minutes (Figure 3).

Li_6WO_6 displays an initial carbonation capacity ∼70% of the theoretical capacity, and the sorption capacity decreases steadily as the material is cycled (Figure 4). By the 25th cycle, the CO_2 sorption capacity is ∼35% of the theoretical capacity. The first cycle has an anomalous sorption capacity because some of the material was likely partially carbonated prior to the experiment, as Li_6WO_6 spontaneously carbonates in ambient conditions. Despite the steady degradation in sorption capacity as the material is cycled, Li_6WO_6 demonstrates impressive carbonation kinetics; the material reaches maximum capacity in less than 1 minute, with no change upon repeated cycling.

Li_4WO_5 displays poor CO_2 sorption capacity compared to its theoretical capacity, but exhibits the most stable gravimetric capacity of all the materials studied here (Figure 4). Li_4WO_5 maintains a steady capacity of ∼20% out to 25 cycles studied here, and the carbonation kinetics improve as the material is cycled. Whereas in the first cycle after 5 minutes of exposure to CO_2 only ∼6% of the

TABLE III. Theoretically derived carbonation reaction parameters for the preliminary candidates selected for this study compared to the values obtained from TGA experiments under $p_{CO_2} = 1 \times 10^4$ Pa.

Compound	$T_{carbonation}$ (K)		CO_2 capacity ($g_{CO_2}/g_{sorbent}$)	
	Screening	Experimental	Screening	Experimental
Li_5SbO_5	781	890	0.186	0.151
Li_6MnO_4	846	840	0.822	0.352
Li_6ZnO_4	817	810	0.772	0.638
Li_4WO_5	503	500	0.151	0.031
Li_6WO_6	1005	880	0.137	0.058

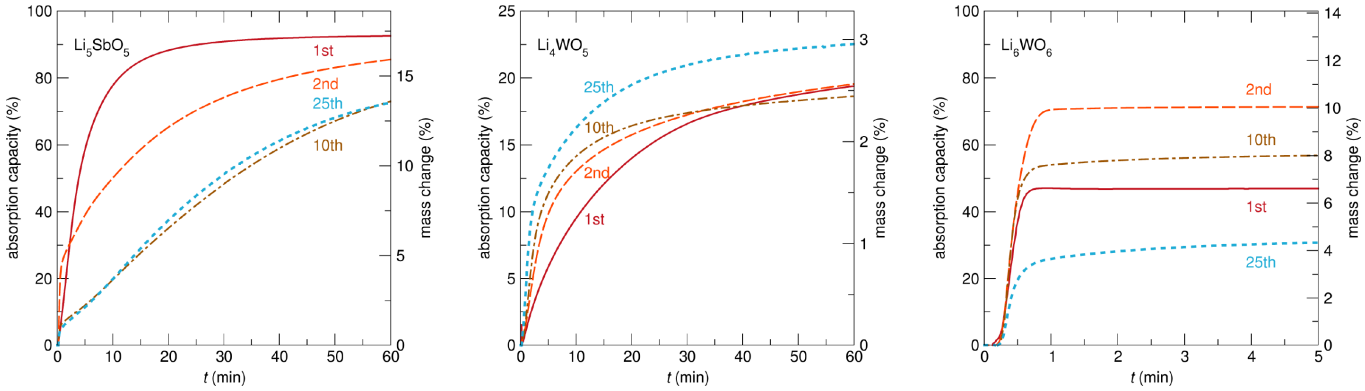

FIG. 3. Selected carbonation profiles for Li_5SbO_5, Li_4WO_5 and Li_6WO_6 from extended carbonation cycling experiments. Both Li_5SbO_5 and Li_6WO_6 show a decrease in capacity after 25 cycles, with Li_5SbO_5 in particular showing a much flatter absorption profile. Li_4WO_5 retains both its profile and capacity for the duration of the cycling, albeit with the lowest capacity of the three materials.

theoretical sorption capacity is reached, after 25 cycles this is doubled; Li_4WO_5 absorbs 13% of the theoretical capacity after the same exposure time (5 min).

D. Structural and morphological evolution of Li_5SbO_5 upon cycling

Li_5SbO_5 was found to be the material with the most promising thermodynamics of carbonation and capacity retention, so it was subjected to further in-depth structural and morphological characterisation to examine changes as a function of cycle number. Samples were extracted at different points in the cycling experiment and analysed using XRD and scanning electron microscopy (SEM). The resulting diffractograms were analysed and the phase fractions in the regenerated material were determined through Rietveld refinement (Figure 5). Diffractograms and fits are available in the Supporting Information.

The phase composition of Li_5SbO_5 after cycling remains relatively stable up to at least three cycles, and is a mixture of ∼83–86 wt.% Li_5SbO_5, ∼12–15 wt.% Li_3SbO_4 and ∼2–3 wt.% Li_7SbO_6 (Figure 5). The formation of a secondary phase with a higher lithium content upon regeneration is surprising considering this behaviour has never been seen for other similar materials, but may play a role in the stable cycling capacity observed for the material. In addition to the formation of Li_7SbO_6, there is also significant formation of Li_3SbO_4, which does not react upon regeneration under inert atmosphere at higher temperature. TGA experiments on single-phase Li_3SbO_4 prepared separately indicate this phase is inert with respect to carbonation (see Supporting Information), so this represents a permanent loss in capacity, as seen in the cycling TGA experiments discussed earlier.

The phase composition of Li_5SbO_5 eventually does evolve with repeated cycling, and after 26 carbonation cycles the fraction of Li_5SbO_5 formed upon regeneration decreases to 55 wt.%. However, Li_7SbO_6 is formed in a much greater proportion (21 wt.%) than in the early cycles, and is present in roughly the same proportion as Li_3SbO_4 (24 wt.%). The higher lithium content in Li_7SbO_6 decreases the stability of the phase with respect to CO_2, so unlike Li_3SbO_4, we expect Li_7SbO_6 to be much more reactive to CO_2. Consequently, although the fraction of the original phase being regenerated decreases with increased cycling, the capacity of "Li_5SbO_5" as a material remains relatively stable due to the formation of Li_7SbO_6.

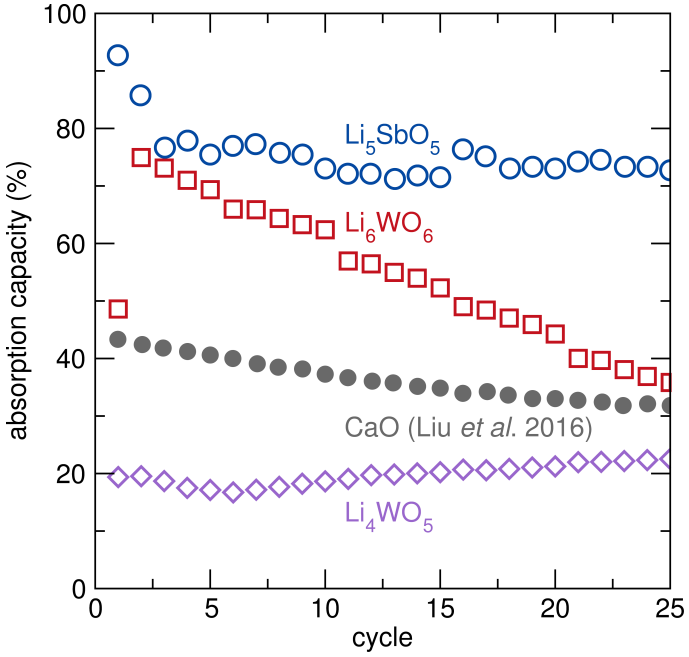

FIG. 4. The percentage absorption capacity measured for each of Li_5SbO_5, Li_6WO_6 and Li_4WO_5 over the 25 carbonation and regeneration looping cycles. Li_5SbO_5 displays sustained capacity retention after the first 3 cycles; Li_4WO_5 actually shows an increase in capacity overall. The Li_6WO_6 displays less favourable looping behaviour, with a steady loss in capacity from cycle 2 onwards. The results for CaO were calculated using data courtesy of Liu *et al.*[20] and have been included for comparison.

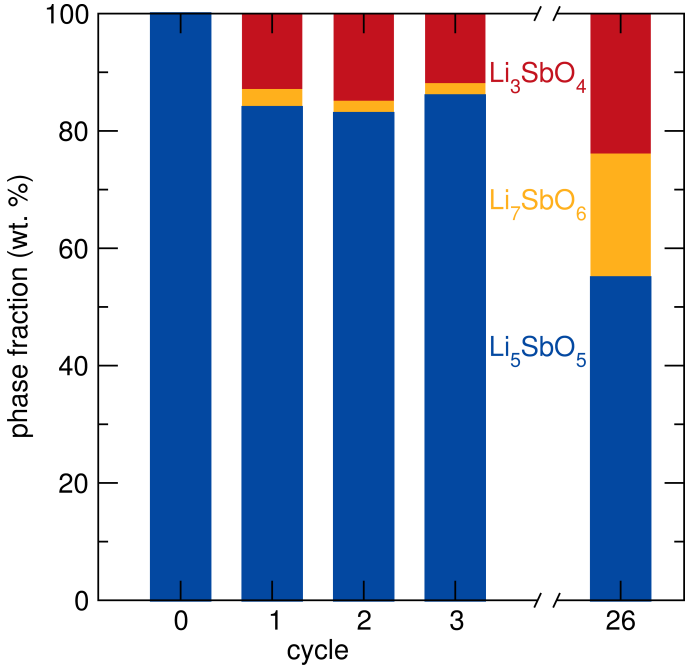

FIG. 5. Phase fraction evolution of regenerated Li_5SbO_5 as a function of cycle number, as determined by Rietveld refinement. Upon repeated carbonation cycles, less Li_5SbO_5 is formed upon regeneration, but overall CO_2 sorption capacity is unchanged due to the formation of unreactive Li_3SbO_4 and reactive Li_7SbO_6.

The SEM micrographs, shown in Figure 6, also give an insight into the microstructural evolution of Li_5SbO_5 upon cycling. After the first carbonation step, the formation of Li_2CO_3 can be seen in the apparent coarsening of the Li_5SbO_5 particles, in line with the observations in previous SEM experiments of carbonated materials such as Na_3SbO_4.[15] This surface area is recreated upon regeneration, and the image at higher magnification shows that the finer structural features on the surface of the particles are also regenerated. Crucially, the images taken at the same point in the carbonation cycle after 26 cycles show a similar surface area and size of the secondary particles. The primary particles are larger and less fused together following multiple cycles, which supports the stable cycling capacity seen in the material.

E. Discussion

The benefit of a large scale screening is that it allows broader insight into trends and underlying causes of observed physical properties. This study is the latest in a growing body of work experimentally characterising the CO_2 absorption properties of promising ternary oxides, and the results can be compared to previous work to better understand the key factors in carbonation reactions.

We examine the role of metal ion and crystal structure by comparing alkali transition metal oxides adopting the antifluorite-type structure. These phases have similar crystal structures and compositions, and differ primarily in the identity of the transition metal in the material. The materials include Li_6MnO_4, Li_6ZnO_4, and Li_6CoO_4 (studied in this work), as well as Li_5FeO_4[15] and Li_5AlO_4.[12] These materials all show remarkably similar carbonation profiles, with the onset of a small initial mass gain at low temperature around ∼600 K, followed by a sharp onset and substantial mass gain at higher temperatures initiated between 850 K and 900 K. This is sensible given the carbonation reactions of these materials calculated in this work have very similar ΔE^{DFT}, with values ranging from −2.16 eV to −2.32 eV. This family of materials display similar carbonation capacities, with experimental values ranging from 82% of theoretical capacity for Li_6CoO_4 studied in this work, to 96% for Li_5AlO_4.[12]

Looking across these lithium-rich antifluorite-type materials, the choice of metal in these materials is not critical, and given the reasonable carbonation properties across the family, targeting specific structure types may be an efficient and fruitful direction for future rational design. Here, the thermodynamic driving force and high capacities are enabled by the high lithium content. Meanwhile, the good kinetics and remarkably fast

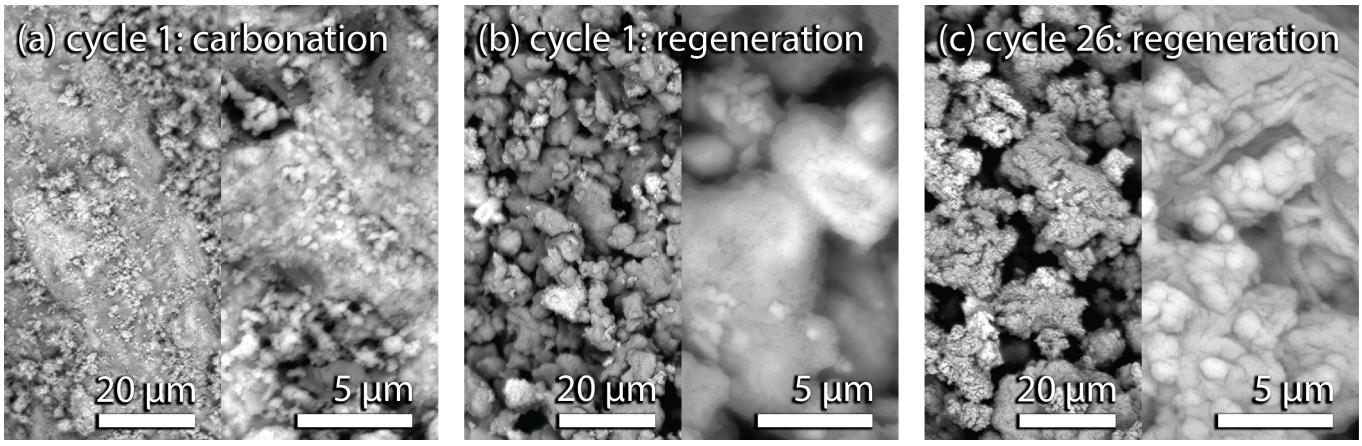

FIG. 6. Scanning electon micrographs of Li_5SbO_5 after (a) the 1st carbonation, (b) the 1st regeneration, and (c) the 26th regeneration. Both regenerated specimens display similar morphology and no sign of coarsening, suggesting the microstructure is conserved upon repeated cycling.

CO_2 absorption seen at higher temperatures are likely enabled by the many partially-occupied Li sites in the crystal structure, which lead to high rates of Li transport through the material once defect-mediated transport mechanisms are activated.

Despite the promising CO_2 sorption capacities and rates, this study found Li_6MnO_4 and Li_6ZnO_4 could not be regenerated and hence cycled, in a similar fashion to the related materials Li_5FeO_4 and Li_6CoO_4.[15] Other methods will thus be required to make these materials appropriate for looping applications. One strategy that has been shown to be successful is the inclusion of water vapour in the reactant gas stream which led to a significant decrease in the temperature required for regeneration of Li_5AlO_4.[21] A similar strategy that shifts the carbonation equilibrium temperature may very well work with the entire class of antifluorite materials, and future work is planned to investigate this and the overall role water plays in CO_2 absorption and regeneration cycles.

The surprising cycling behaviour of Li_5SbO_5 and the formation of increasing amounts of the over-lithiated phase Li_7SbO_6 opens a new route towards finding new ternary systems that maintain their cycling capacity. Instead of relying upon complete regeneration of the original material, if there are other phases with similar composition and reactivity that can be accessed during the reaction, their creation can counteract the loss of capacity caused by coarsening and the permanent formation of inert phases. Furthermore the SEM images indicate that Li_7SbO_6 may indeed form with similar morphology as the original Li_5SbO_5 phase, leading to little decline in reactivity with cycling. The fact these phases might be metastable (Li_7SbO_6 lies 0.008 eV above the hull in the Li–Sb–O phase diagram calculated by the Materials Project) means future screenings should include metastable materials close to the hull, otherwise potential reaction pathways that can be accessed under carbonation cycling conditions might be missed.

As seen in previous studies on $Ba_4Sb_2O_9$,[14] conservation of capacity and morphology are strongly linked, a phenomenon that is the subject of ongoing analysis and effort to also include in future screening methodologies. The SEM of Li_5SbO_5 further supports these earlier studies, even if the underlying causes for microstructure retention are not known. There is nevertheless a degradation in the absorption rate of Li_5SbO_5 as the material is cycled, which is an opportunity for future studies aimed at achieving capacity retention rates comparable to those obtained following steam injection in the CaO system.[22–24]

The absolute capacity of Li_4WO_5 is the lowest amongst the materials in this study, and would certainly require larger amounts of material to be used in CCS applications, but this is not necessarily an insurmountable barrier to its implementation. Li_4WO_5 is predominantly composed of Li–O, with a low loading of W. Consequently, the total mass needed to achieve a certain gravimetric CO_2 absorption value would be comparable to heavier materials with better capacities, such as Li_5SbO_5 or $Ba_4Sb_2O_9$. Furthermore, certain CCS applications do not require particularly high capacities. In particular, CCS applications on a smaller scale than power generation, such as improving hydrogen yields in chemical looping processes[25] or chemical looping partial oxidation of methane,[26] rely on efficient and complete regeneration over many cycles, properties displayed by Li_4WO_5. This finding highlights the advantage of large scale screening methods in that materials can be found for different target applications in the same experiment, and further selected on various criteria.

A final interesting observation arising from the screening comes when considering the materials that were predicted to carbonate but failed to do so in experiments. This group of materials had low predicted tem-

peratures of carbonation, where under atmosphere of $p_{CO_2} < 1 \times 10^5$ Pa, $T_{\text{carbonation}} \lesssim 600$ K: $CaWO_4$ (323 K), Li_2WO_4 (503 K), $Ca_4Nb_2O_9$ (606 K), Li_3NbO_4 (503 K), Li_3TaO_4 (511 K) and Li_3SbO_4 (532 K). Considering the earlier studies investigating the connection between carbonation and ionic mobility,[27–29] these results suggest a material may not carbonate at low temperatures due to insufficient ionic mobility, even if a material is predicted to carbonate based on thermodynamics. As the temperature is increased into a region where ionic mobility might be sufficient, the equilibrium may favour regeneration (*i.e.*, decarbonation) rather than carbonation, leading to further inactivity.

The need to balance two competing factors for the development of successful CCS materials is important for future studies. The carbonation temperature must be low enough to avoid particle coarsening, which leads to loss of capacity as in the pure CaO-$CaCO_3$ system. However, the carbonation temperature cannot be so low as to hinder ionic diffusion in the material and cause slow carbonation kinetics. This also explains the anomalous materials that carbonate at low temperature: owing to the smaller ionic radius and charge of Li^+ when compared to Ca^{2+}, one would expect faster ionic diffusion in Li_4WO_5 at lower temperatures than Ca analogues (*e.g.*, $CaWO_4$ and Ca_3WO_6), and hence we observe some carbonation of Li_4WO_5 even at the low temperatures where the Ca-based materials do not react. The difficulty in achieving sufficient Ca ionic diffusion means that even with a reasonably high carbonation temperature the reaction does not occur. Thus, thermodynamic screening needs to be carried out in concert with screening for ionic diffusivity, a methodology that is the focus of ongoing work. Focusing only on decreasing the energy penalty of the chosen material needs to be balanced with other parameters that influence actual performance.

IV. CONCLUSIONS

In this study we used the theoretical screening of structural databases as a starting point for exploring novel materials for use in high-temperature carbon capture and storage (CCS) applications. Diverse candidate materials were selected, and either displayed desirable theoretical properties or allowed direct compositional and/or structural comparisons to previously studied materials. These candidates were subjected to a suite of structural and thermogravimetric experiments to determine their performance as CO_2 looping materials.

In the first instance, this initial testing reveals that the theoretical screening accurately predicts the carbonation temperature of the candidate materials studied here, but fails to identify materials whose carbonation is hindered by poor kinetics. Li_5SbO_5, Li_6WO_6 and Li_4WO_5 all exhibit reversible CO_2 sorption, with Li_5SbO_5 showing a particularly high and stable capacity retention over 25 carbonation cycles. Li_5SbO_5 has a stable microstructure that is preserved through repeated cycling; scanning electron micrographs of "Li_5SbO_5" after regeneration do not reveal any significant evolution of morphology after 25 cycles. Further structural analysis at different stages of cycling reveals the formation of a secondary metastable phase upon reaction, Li_7SbO_6, which may prevent coarsening and deactivation of the sorbent. This phase space, where there are many easily accessible stoichiometries upon reaction that are close in energy, could prove fertile ground for the design of new robust CCS materials.

Further analysis of the candidate materials studied here in concert with the body of previous research carried out by authors in this work hint at other important design principles for future research, the most crucial being the need to use a moderate temperature to satisfy both energetic and diffusion considerations in CO_2 absorption materials. The design of new materials, as well as the chemical and structural modification of exisiting materials, need to consider these two factors to find a suitable reaction temperature that has favourable thermodyanamic driving force as well as sufficiently fast ionic transport. The performance of materials in CCS applications is the result of a delicate balance between thermodynamics, ion diffusion, and morphology, and requires a similarly balanced mix of theoretical, synthetic and analytical approaches to fully understand how to harness these competing forces.

ACKNOWLEDGMENTS

The authors thank Zlatko Sarakevic for carrying out the BET experiments, and Wen Liu, Stuart Scott and John Dennis for fruitful discussions regarding the work and assistance with the TGA experiments. The authors also gratefully acknowledge Anubhav Jain (Computational Research Division, Lawrence Berkeley National Laboratory), Shyue Ping Ong (Department of NanoEngineering, University of California San Diego) and Kristin Persson (Department of Materials Science and Engineering, University of California Berkeley) for their advice and assistance in accessing the Materials Project, which itself is supported through the U.S. Department of Energy, Office of Basic Energy Sciences, Materials Project Center Grant No. EDCBEE. MWG is grateful for support from the European Union's Horizon 2020 research and innovation programme under the Marie Skłodowska–Curie grant agreement No. 659764. MTD and CPG acknowledge funding from EPSRC Grant No. EP/K030132/1. MTD is grateful for support from Clare College, Cambridge through the award of a Junior Research Fellowship.

V. DATA

All supporting data for this work can be found on https://www.repository.cam.ac.uk.

VI. SUPPORTING INFORMATION

XRD diffractograms and Rietveld refinements for the candidate materials, surface area measurements, XRD diffractograms of Li_5SbO_5 at different stages of carbonation cycle, and TGA traces for candidate materials. This material is free of charge via the Internet at http://pubs.acs.org.

REFERENCES

[1] A. D. Ebner and J. A. Ritter, "State-of-the-art adsorption and membrane separation processes for carbon dioxide production from carbon dioxide emitting industries," Separ. Sci. Technol. **44**, 1273–1421 (2009).

[2] D. P. Hanak, E. J. Anthony, and V. Manovic, "A review of developments in pilot-plant testing and modelling of calcium looping process for CO_2 capture from power generation systems," Energy Environ. Sci. **8**, 2199–2249 (2015).

[3] A. M. Kierzkowska, R. Pacciani, and C. R. Müller, "CaO-based CO_2 sorbents: From fundamentals to the development of new, highly effective materials," ChemSusChem **6**, 1130–1148 (2013).

[4] E. Bouquet, G. Leyssens, C. Schönnenbeck, and P. Gilot, "The decrease of carbonation efficiency of CaO along calcination–carbonation cycles: Experiments and modelling," Chem. Eng. Sci. **64**, 2136–2146 (2009).

[5] K. Nakagawa and T. Ohashi, "A novel method of CO_2 capture from high temperature gases," J. Electrochem. Soc. **145**, 1344–1346 (1998).

[6] K. Nakagawa and T. Ohashi, "A reversible change between lithium zirconate and zirconia in molten carbonate," Electrochem. **67**, 618–621 (1999).

[7] A. López-Ortiz, N. G. P. Rivera, A. R. Rojas, and D. L. Gutierrez, "Novel carbon dioxide solid acceptors using sodium containing oxides," Sep. Sci. Technol. **39**, 3559–3572 (2004).

[8] T. Zhao, E. Ochoa-Fernández, M. Rønning, and D. Chen, "Preparation and high-temperature CO_2 capture properties of nanocrystalline Na_2ZrO_3," Chem. Mater. **19**, 3294–3301 (2007).

[9] T. Yamaguchi, T. Niitsuma, B. N. Nair, and K. Nakagawa, "Lithium silicate based membranes for high temperature CO_2 separation," J. Membr. Sci. **294**, 16–21 (2007).

[10] M. J. Venegas, E. Fregoso-Israel, R. Escamilla, and H. Pfeiffer, "Kinetic and reaction mechanism of CO_2 sorption on Li_4SiO_4: Study of the particle size effect," Ind. Eng. Chem. Res **46**, 2407–2412 (2007).

[11] T. Ávalos-Rendón, J. Casa-Madrid, and H. Pfeiffer, "Thermochemical capture of carbon dioxide on lithium aluminates ($LiAlO_2$ and Li_5AlO_4): A new option for the CO_2 absorption," J. Phys. Chem A **113**, 6919–6923 (2009).

[12] T. Ávalos-Rendón, V. H. Lara, and H. Pfeiffer, "CO_2 chemisorption and cyclability analyses of lithium aluminate polymorphs (α- and β-Li_5AlO_4)," Ind. Eng. Chem. Res **51**, 2622–2630 (2012).

[13] H. A. Lara-García, P. Sanchez-Camacho, Y. Duan, J. Ortiz-Landeros, and H. Pfeiffer, "Analysis of the CO_2 chemisorption in Li_5FeO_4, a new high temperature CO_2 captor material. effect of the CO_2 and O_2 partial pressures," J. Phys. Chem. C **121**, 2455–3462 (2017).

[14] M. T. Dunstan, W. Liu, A. F. Pavan, J. A. Kimpton, C. D. Ling, S. A. Scott, J. S. Dennis, and C. P. Grey, "Reversible CO_2 absorption by the 6H perovskite $Ba_4Sb_2O_9$," Chem. Mater. **25**, 4881–4891 (2013).

[15] M. T. Dunstan, A. Jain, W. Liu, S. P. Ong, T. Liu, J. Lee, K. A. Persson, S. A. Scott, J. S. Dennis, and C. P. Grey, "Large scale computational screening and experimental discovery of novel materials for high temperature CO_2 capture," Energy Environ. Sci. **9**, 1346–1360 (2016).

[16] D. Cruz, S. Bulbulian, E. Lima, and H. Pfeiffer, "Kinetic analysis of the thermal stability of lithium silicates (Li_4SiO_4 and Li_2SiO_3)," J. Solid State Chem. **179**, 909–916 (2006).

[17] A. A. Coelho, "*TOPAS* and *TOPAS-Academic*: An optimization program integrating computer algebra and crystallographic objects written in C++," J. Appl. Crystallogr. **51**, 210–218 (2018).

[18] S. Brunauer, P. H. Emmett, and E. Teller, "Adsorption of gases in multimolecular layers," J. Am. Chem. Soc. **60**, 309–319 (1938).

[19] J. Hauck, "Zur kristallstruktur des Li_6WO_6," Z. Naturforsch. B **24**, 251 (1969).

[20] W. Liu, B. González, M. T. Dunstan, D. S. Sultan, A. Pavan, C. D. Ling, C. P. Grey, and J. Dennis, "Structural evolution in synthetic, Ca-based sorbents for carbon capture," Chem. Eng. Sci. **139**, 15–26 (2016).

[21] T. L. Ávalos-Rendón and H. Pfeiffer, "High CO_2 chemisorption in α-Li_5AlO_4 at low temperatures (30–80°C): Effect of the water vapor addition," Energy Fuels **26**, 3110–3114 (2012).

[22] V. Nikulshina, M. E. Gálvez, and A. Steinfeld, "Kinetic analysis of the carbonation reactions for the capture of CO_2 from air via the $Ca(OH)_2$–$CaCO_3$–CaO solar thermochemical cycle," Chem. Eng. J. **129**, 75–83 (2007).

[23] V. Manovic and E. J. Anthony, "Carbonation of CaO-based sorbents enhanced by steam addition," Ind. Eng. Chem. Res **49**, 9105–9110 (2010).

[24] I. Lindén, P. Backman, A. Brink, and M. Hupa, "Influence of water vapor on carbonation of CaO in the temperature range 400–550°C," Ind. Eng. Chem. Res **50**, 14115–14120 (2011).

[25] M. S. C. Chan, W. Liu, M. Ismail, Y. Yang, S. A. Scott, and J. S. Dennis, "Improving hydrogen yields, and hydrogen:steam ratio in the chemical looping production of hydrogen using $Ca_2Fe_2O_5$," Chem. Eng. J. **296**, 406–411 (2016).

[26] S. Bhavsar and G. Veser, "Chemical looping beyond combustion: Production of synthesis gas via chemical looping partial oxidation of methane," RSC Adv. **4**, 47254–47267 (2014).

[27] J.-i. Ida and Y. S. Lin, "Mechanism of high-temperature CO_2 sorption on lithium zirconate," Environ. Sci. Technol. **37**, 1999–2004 (2003).

[28] M. T. Dunstan, J. M. Griffin, F. Blanc, M. Leskes, and C. P. Grey, "Ion dynamics in Li_2CO_3 studied by solid-state NMR and first-principles calculations," J. Phys. Chem. C **119**, 24255–24264 (2015).

[29] M. T. Dunstan, H. Laeverenz Schlogelhofer, J. M. Griffin, M. S. Dyer, M. W. Gaultois, C. Y. Lau, S. A. Scott, and C. P. Grey, "Ion dynamics and CO_2 absorption properties of Nb-, Ta-, and Y-doped Li_2ZrO_3 studied by solid-state NMR, thermogravimetry, and first-principles calculations," J. Phys. Chem. C **121**, 21877–21886 (2017).

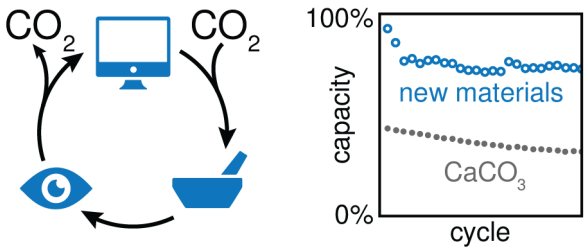

TOC graphic